Bellowband: A Pneumatic Wristband for Delivering Local Pressure and Vibration

Eric M. Young[†‡], Amirhossein H. Memar[†], Priyanshu Agarwal[†], and Nick Colonnese[†]

***Abstract*— In this paper we present the design and control of Bellowband, a pneumatic wristband for localized pressure and vibration haptic feedback. The wristband has eight equally spaced pneumatic bellows that extend into the wrist, constructed from layers of polyester thermoplastic polyurethane (TPU), resulting in a flexible, lightweight (11 g) band capable of rendering complex pressure and vibration cues to the user. Each bellow can withstand over 100 kPa, extend over 10 mm, and exert over 10 N of force at zero displacement. Quasi-static analysis is performed to estimate bellow force for a given input pressure and bellow displacement, and the dynamic response is examined experimentally. Finally, we demonstrate the wristband's ability to deliver various haptic cues to the wrist, including uniform squeeze, uniform vibration, local force, and local vibration. Bellowband is a thin, soft, low-encumbrance wristband that can provide meaningful haptic feedback, making it ideal for AR/VR environments.**

I. Introduction

Realism and intuitive feedback can contribute to high quality Augmented Reality (AR) and Virtual Reality (VR) interaction. There have been various efforts to broaden and streamline the information transfer to the user associated with physical interaction in virtual and augmented worlds. Many AR/VR systems rely on handheld controllers to track hand pose and provide familiar input interfaces such as buttons and joysticks. Although beneficial for tracking and ease of use, these controllers provide limited haptic feedback and inherently obstruct free motion of the user's hands. Other systems use bare-hands-tracking to remove the need for handheld controllers. In doing so, such systems allow a user to more seamlessly switch between manipulating real and virtual objects, but forfeit the additional information that haptic feedback provides. Particularly in AR environments, there is a growing need to keep the hands free to interact with physical objects while providing meaningful haptic feedback for interaction with virtual objects.

One potential solution is to design a fingertip device or glove that is sufficiently haptically transparent. Many fingertip [1] and glove [2] designs have been explored, but so far these devices face challenges with being too encumbering or haptically opaque to allow natural interaction with physical world objects. An alternative approach is to relocate haptic feedback to another part of the body, such as the wrist. Haptic wristbands promise to keep the user's hands free, and may also prove to be a practical alternative to more direct haptic interfaces, such as gloves. Haptic wristbands exist for various applications, but the deliverable haptic cues have been predominately limited to vibration.

[†]Facebook Reality Labs, Redmond, WA 98052, USA. [‡]Haptics Group, Dept. of Mechanical Engineering and Applied Mechanics, University of Pennsylvania, Philadelphia, PA 19104, USA.

Fig. 1: Bellowband is a pneumatic wristband that can deliver local pressure and vibration at eight positions around the wrist. The device is made from thermoplastic polyurethane (TPU), resulting in a lightweight wristband capable of rendering complex pressure and vibration to the user.

In this paper we present a pneumatic wristband that is capable of providing haptic feedback in the form of local vibration and pressure around the user's wrist. We make contributions in the following two areas: increasing functionality through the inclusion of eight independent actuators that can deliver both vibration and analog pressure, and increasing wearability through the use of pneumatics and soft, lightweight materials. First, in Section II we discuss relevant prior work relating to both wristband haptics and pneumatic actuation. Then, in Section III, we present the general design of our pneumatic haptic wristband and manufacturing methods. In Section IV we characterize the bellow actuators and evaluate quasi-static force and response time across the workspace. Section V gives an overview of the types of haptic cues the wristband can deliver, and Section VI concludes and presents future work.

II. Prior Work

Vibrotactile feedback can be cheaply and effectively implemented, leading many haptic wristband designs to rely solely on vibration to communicate with the wearer. Studies aimed at maximizing information transfer via vibration have shown that localization rate can be improved by spreading vibrotactors across rather than along the forearm [3]–[5], and increasing the number of tactors around the wrist up to eight

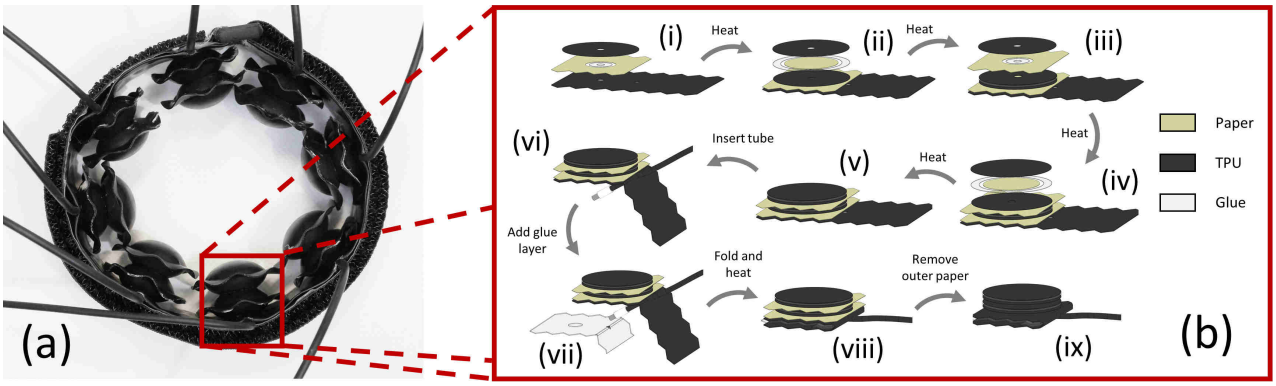

Fig. 2: The final device with all bellows pressurized is shown in (a), and the manufacturing process for a single bellow is shown in (b). In steps (i)-(v), alternating layers of TPU and glue are stacked to form two internal pockets that extend upward when pressurized. A tube is inserted into the base layers of TPU and glue in steps (vi)-(vii). In step (viii) the tube is positioned beneath the hole to allow airflow to the bellow and glued into place. Finally the outer paper layers, used to facilitate the separation of non-glued TPU layers, is removed in step (ix). The inner paper layers remain inside the bellows.

[6]. All of these vibrotactile wristbands are lightweight and can deliver valuable information to the user, but they are unable to provide other haptic cues such as localized force or squeeze.

Additional work has explored providing uniform squeeze via a single servo motor [7]–[9], squeeze and shear via two motors [10], or squeeze, shear, and vibration via combinations of motors and vibrotactors [11], [12]. However, these wristbands have limited degrees of freedom and each servo motor adds significant weight to the wrist. Pneumatic systems can reduce the weight required to render uniform squeeze [13], [14], but these systems are still limited to a few degrees of freedom. Other devices can apply localized force to the wrist through electro-mechanical means [7], [15], but these need a motor for each force location, requiring significant space and weight to deliver multiple local forces. Pneumatic approaches have again shown potential to reduce the weight associated with these designs. He et al. designed a wristband with five silicone chambers, but the inflation and deflation times are 4 s and 1 s respectively [16]. Raitor et al. achieved response times of as little as 13 ms for a four-pocket pneumatic wristband that boasted easy fabrication and a low profile, but the maximum pressure of each pocket was limited to 12 kPa [17].

Outside the realm of haptics, much work has been done towards developing lightweight pneumatic linear actuators that are easy to manufacture. Printable lightweight bellow actuators [18] can deliver high forces, but require some non-zero minimum length and are slightly more rigid than other options. Silicone designs have offered more flexible and thin solutions, but often have limited maximum pressures. Furthermore, silicone bubble arrays [19] do not offer the amount of extension we desire, and silicone linear actuators that offer greater displacements [20] still have a non-zero minimum length. Coating or sealing origami structures with an elastomer has shown potential in creating low-profile, strong, flexible actuators [21]–[23]. Pneumatic bellows developed by Ranzani et al. and Becker et al. boast a simplified manufacturing process and have been shown to deliver forces up to 10 N [24], [25]. These bellows were constructed from layers of flexible, lightweight thermoplastic elastomers, making them viable candidates for implementation into a haptic wristband.

III. Device Design

Our wristband design was largely inspired by prior work in the field, namely that up to eight actuators can improve localization and that thermoplastic elastomers can be layered to form robust, yet simple, pneumatic actuators.

A. Design Goals

Our goal was to render meaningful haptic cues through a minimally encumbering design. With respect to meaningful haptic cues, we aimed to deliver independent vibrotactile and constant force cues around the wrist, allowing lower-dimensional haptic feedback, such as squeeze, as well as higher-dimensional cues such as multi-point force and vibration. Preliminary internal testing suggested that 5 N force delivered by a 15 mm indenter gave a strong haptic sensation without causing pain, and required displacements up to 6 mm at softer positions around the wrist. We thus aimed to have each bellow of Bellowband deliver 5 N of force at 6 mm of displacement. However, more work is needed to select maximum forces and corresponding displacements that are ideal for the general population. We also wanted to enable vibration of at least 5 Hz, as Raitor et al. reported that users could identify the location of 5 Hz vibrotactile cues delivered by a four-pocket pneumatic wristband with over 99% accuracy [17].

With respect to encumbrance, we wanted to minimize weight and maximize comfort. A key benefit of using pneumatic actuation is the ability to move heavier components, such as valves, regulators, and compressors, to a remote location. Although there is still some encumbrance associated transmitting pneumatic power via small tubes, the resulting systems can be low weight and low volume, but can deliver high forces. We wanted to maintain this inherent low encumbrance by using lightweight, flexible materials and limiting the wristband to a weight of 15 g and a width of 20 mm.

B. Mechanical Design

Bellowband consists of a series of eight independent actuators located around the wrist. We used a bellow design

for the actuators, in which rings of polyester thermoplastic polyurethane (polyester TPU) are sealed at the boundaries, creating air pockets between sequential rings. When air pressure is supplied to these internal pockets, the pockets extend along an axial direction, causing displacement and/or contact force to increase. The glue used to seal adjacent TPU rings is also a polyester TPU, but has a lower melting temperature. For ease of discussion, we will refer to the melting TPU as "glue", and the structural TPU as "TPU".

The wristband is assembled one layer at a time, alternating between glue and TPU, as shown in Fig. 2. After each layer of TPU, the entire wristband is pressed at 140 kPa and 260° F for 30 seconds. The wristband has a nearly inextensible outer strip of nylon, from which the eight equally spaced bellows extend inward toward the center of the wrist. The bellows are spaced 24 mm apart, resulting in a maximum allowed wrist circumference of 192 mm. Air pressure is supplied to each bellow via tube inserts beneath the bellows. Ethylene propylene diene monomer (EPDM) rubber tubing with 1/32" inner diameter runs to each bellow and a small segment of stainless steel tubing with 0.032" OD and 0.025" ID is glued into the end of the EPDM, to prevent the tube from sealing when pressed. The entire band, including a sewn on hook and loop material for fastening, weighs under 11 g. Note that heavier pneumatic components are required to power and control the system, but that these components are not worn by the user.

C. System Design

Sections IV and V feature slightly different setups for data collection, but use nearly the same components. Both setups actuate a bellow using a Kelly Pneumatics Inc. high flow pressure regulator, a 64 oz. air chamber, and a Parker C7 miniature cartridge valve. Although the locations of sensors vary by application, both setups include Cynergy3 IPSU-GP100-6 pressure sensors, and an ATI Nano17 six-axis force/torque sensor. A flowchart of the pneumatic components is shown in Fig. 3.

To control a bellow actuator, we first set the regulator to the desired pressure, P_{des}, and feed its output to the input of the high-speed valve. The valve output is connected to the bellow, allowing us to alternate the bellow pressure between P_{des} and atmospheric pressure, P_{atm}. We originally had the regulator output directly to the valve, but early tests showed a two-part response: first a quick pressure rise corresponding to the valve opening, and a second, more gradual pressure rise

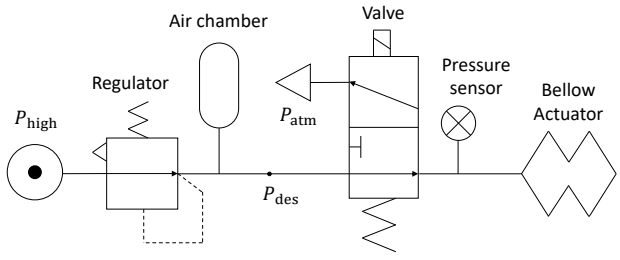

Fig. 3: Schematic of the pneumatic components for each bellow. Controlling the entire wristband requires eight identical, independent setups.

as the regulator compensated for the airflow to the bellow. We were able to eliminate the second rise associated with the regulator by adding an air chamber between the regulator and the valve. Although this reservoir decreases the response time of the system to a change in P_{des}, it allows us to better separate the response of the physical bellow from the response of the pneumatic control. This setup allows us to achieve step responses on the order of 10 ms using the valve, and analog pressure control on the order of seconds using the regulator. Sensor measurements for both setups are recorded at over 1000 Hz, including pressure between the valve and the bellow and force/torque exerted by the bellow.

IV. Bellow Characterization

In this section we present data from various bellow designs to provide an overview of the design space and justify our final selection of design parameters. We then provide a simple spring model for our selected bellow design, in order to accurately predict the response under various conditions.

A. Bellow Design Parameters and Characterization Setup

In a general TPU bellow design, each layer can have a unique 2D geometry or material type, resulting in a large design space. In this discussion, we restrict our design space to circular bellows with the same TPU material used throughout, although we would like to test different layer geometries in the future. Five parameters define the resulting design space: inner radius r_i, outer radius r_o, glue width w, TPU thickness b, and number of pockets n, as shown in Fig. 4. Some of these parameters are restricted by our design goals and manufacturing methods; to achieve maximum bellow displacement, we want to minimize inner radius, minimize glue width, and maximize outer radius. The remaining parameters to explore are the number of pockets, n, and the TPU thickness, b.

We constructed bellows with combinations of n and b shown in Table I and measured the force output at various pressures and displacements for each design. We first fixed the base of the bellow and set the distance of a flat plate attached to the force sensor, x_{plate}, as shown in Fig. 5(a). We then commanded the pressure regulator to P_{des} and paused

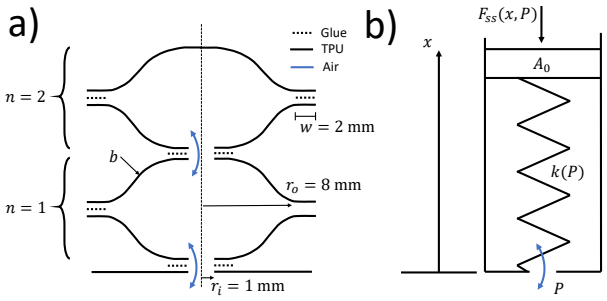

Fig. 4: (a) shows bellow design parameters. Each bellow consists of stacked, glued TPU pockets of a circular geometry. A lower limit of 1 mm for the inner radius to allow airflow, an upper limit of 20 mm for overall wristband width, and inconsistent seals for glue widths less than 2 mm led us to define inner radius $r_i = 1$ mm, outer radius $r_o = 8$ mm, and glue width $w = 2$ mm. TPU thickness, b, and number of pockets, n, were determined experimentally. (b) shows our variable spring model for quasi-static force exerted by a bellow.

TABLE I: Bellow Design Parameters and Performance

n	1	1	1	2	2	2	3	3	3
b (µm)	38	76	178	38	76	178	38	76	178
$P_{\max}$ (kPa)	34	69	103	34	69	103	34	69	103
$L_{\max}$ (mm)	7	6	6	11	12	10	18	18	16
$F_{\max}$ at 6 mm (N)	0.1	0.0	0.7	1.7	4.3	5.0	3.0	5.7	8.4

The design parameters n and b represent the number of pockets and the TPU thickness respectively. $P_{\max}$ is the maximum pressure we tested for a given material, determined experimentally to be safely below the value at which failure occurs. $L_{\max}$ is free length of the bellow at $P_{\max}$. $F_{\max}$ is the force exerted by the bellow at $P_{\max}$ on a plate 6 mm from the base of the bellow. We selected the two-pocket 178 µm TPU bellow (highlighted) for our wristband, as this was the only bellow with two or fewer pockets to meet our design goal of delivering over 5 N of force at 6 mm displacement.

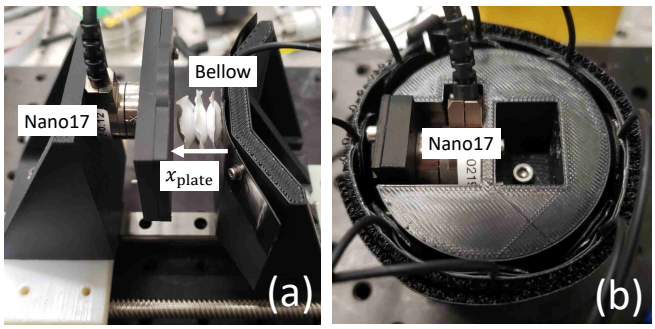

Fig. 5: Two setups for measuring force output of a bellow. Setup (a) is used for bellow characterization (Section IV), where a force-sensing plate is set at a controlled distance from the base of the bellow. Setup (b) is used for full wristband evaluation (Section V). The wristband is placed around a rigid cylinder with a separated force-sensing section located under one bellow, and the wristband can be rotated to measure forces under each of the bellows.

for five seconds to allow the air chamber pressure to stabilize. Next we commanded the valve to supply a step change in pressure and recorded force and pressure measurements for five seconds. A total of three trials were completed for both step increases and step decreases. For each bellow design, we iterated through plate distances from 0 mm to the maximum bellow length in increments of 1 mm, and for each plate distance we iterated through pressures from 0 kPa to a maximum pressure dependent on the material thickness in increments of 6.9 kPa.

As expected, our data shows that bellow designs with more pockets exert more force at a given displacement. However, additional pockets also require more material, making the wristband heavier and less flexible, and also make the bellow more susceptible to motion perpendicular to the axis of extension. The selected design was the only bellow with two or fewer pockets to meet our design goal of delivering over 5 N of force at 6 mm displacement. Our data suggests that future designs with thicker TPU could accommodate an even greater range of force and displacement, but at the cost of greater weight, stiffness, and required pressure.

B. Quasi-static Analysis and Modeling

Force measurements corresponding to all commanded pressures and plate distances for the selected design are shown in Fig. 6. This data suggests that for a given pressure, the force exerted by the bellow varies linearly with displacement. Modeling the system as a spring with a variable

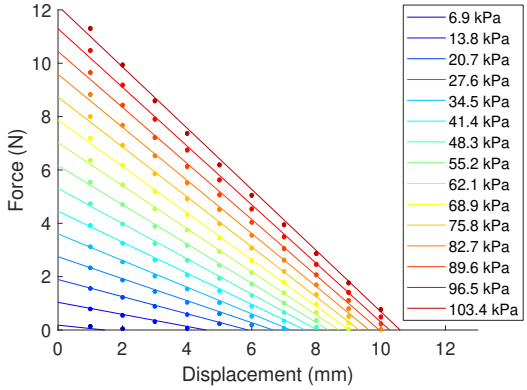

Fig. 6: Measured quasi-static forces exerted by the selected bellow are depicted as dots for all pressures and displacements. The linear relationship between force and displacement for a given pressure suggested a model given by Equations (1)-(3), which is depicted as lines and has an RMS error of 0.11 N.

stiffness dependent on pressure, as shown in Fig 4, gives the following equation for quasi-static force:

$$F_s(x, P) = PA_0 - k(P)x \tag{1}$$

where P [Pa] is the air pressure inside the bellow, x [m] is the displacement of the bellow and in our setup is equal to x_{plate}, F_s [N] is the contact force between the bellow and the plate, and A_0 [m^2] is area of a pocket when flat. Conceptually, this suggests that at a constant pressure P, the bellow exerts a force of PA_0 at zero displacement, and that as the bellow is allowed to lengthen, the TPU acts as a spring being stretched. Furthermore, the stiffness is a function of pressure alone and encompasses complexities such as material stress-strain relationship and 2D-geometries.

We first fit a line to the measured $F_s(x, P_i)$ data shown in Fig. 6 for each pressure P_i, giving us estimates of P_iA_0 and $k(P_i)$. In Fig. 7 we see that estimates of PA_0 and $k(P)$ are well-fit across all pressures by the following equations:

$$k(P) = -4.3 \times 10^{-8}P^2 + 0.015P + 24 \tag{2}$$

$$PA_0 = 1.24 \times 10^{-3}P - 0.67 \tag{3}$$

Plugging these model parameters back into Eq. 1 results in a RMS error of 0.11 N across all tested pressures and distances. Note that the constant term in Eq. 3 is due to the definition of x_0, and suggests the mathematically ideal x_0 was slightly closer to the base of the bellow than was defined during the experimental setup. The proportional term in Eq. 3 estimates A_0 at 124 mm^2, which represents a circle of radius 6.3 mm. Although the specified pocket radius, r_0, was 8 mm, the glue flows when heated during the manufacturing process, causing the actual pocket radius to be smaller than specified.

C. Dynamic Response Analysis

We also evaluated the response of our selected bellow design with respect to time. The forces measured during steps from 0 kPa to 100 kPa at a plate distance of 5 mm is shown in Fig. 8. First, we see that the forces are consistent across all three trials. We also note that there is a delay of 10 ms in the step decrease responses, corresponding to the

valve switch time. The step increase responses have a slightly longer delay of 30 ms, corresponding to the additional time needed to expand the bellow to the plate distance of 5 mm.

To characterize of the response time we fit the measured pressure at the bellow input to an exponential curve of the form

$$P(t) = P_\infty(1 - e^{-(t-t_0)/\tau}) \tag{4}$$

for each step pressure increase, and

$$P(t) = P_0(e^{-(t-t_0)/\tau}) \tag{5}$$

for each step pressure decrease, where t_0 is representative of valve delay. We computed averaged τ across three trials for each combination of plate distance and pressure, and plotted the results (Fig. 9.) We see that all conditions have time constants of under 40 ms, with the system responding more quickly to smaller steps in pressure and smaller displacements.

Finally, we obtained the frequency response of our actuator by setting the plate distance to 0 mm and measuring the actuator force output for commanded square waves of amplitude 100 kPa in pressure. We measured the force response of our actuator for 60 s at input square wave frequencies of 0.1, 0.5, 1, 5, 10, 15, 20 Hz and analyzed the unfiltered data using the fast Fourier transform to obtain the Bode plot in Fig. 10 indicating a force bandwidth of 7 Hz. Although we expect this bandwidth to vary as plate distance changes, due to a different bellow volumes needing to be pressurized, this evaluation provides a preliminary evaluation of the entire system. It is worth noting that even attenuated forces can still be perceived, and although future human studies are needed for detailed analysis, frequencies above 40 Hz can still be felt on the wrist.

V. Wristband Demonstration

The unique characteristics of the bellow actuators can enable complex combinations of pressure and vibration. Our setup to evaluate the wristband is similar to our characterization setup, except with the flat contact surface replaced by a cylindrical surface to mimic a wrist, as shown in Fig. 5(b). The setup only measures normal force under one bellow, but the wristband can be rotated between trials to measure force output by each of the eight bellows for a given haptic cue. Although this setup oversimplifies wrist shape and ignores

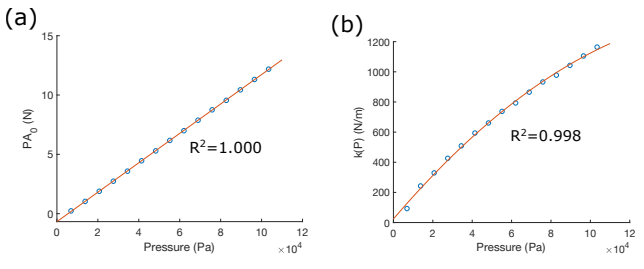

Fig. 7: Data-driven fitting of model parameters of Equation (1), which requires values of PA_0 and $k(P)$. These parameters are functions of bellow geometry and material properties, and were experimentally fit with low-order polynomials. (a) shows the measured values of PA_0 with an affine fit, and (b) shows the measured values of $k(P)$ with a quadratic fit.

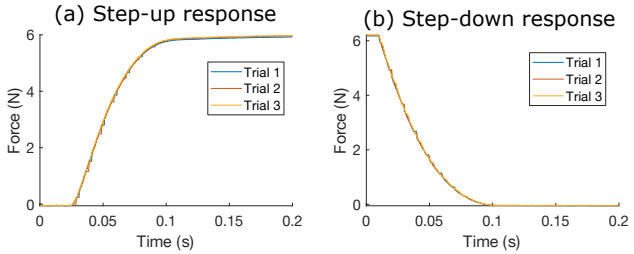

Fig. 8: We measured the force exerted by the bellow during steps from (a) 0 kPa and 100 kPa and from (b) 100 kPa to 0 kPa at a plate distance of 5 mm.

differences in wrist size and deformation of the skin, it is sufficient to demonstrate the types of haptic cues that our system can deliver.

The diagrams in Fig. 11 show examples of forces felt on the wrist during different haptic cues. We see that we are able to effectively deliver local force and vibration, where changes in measured forces are isolated to one of the eight positions, as well as uniform squeeze and vibration, where measured forces change similarly across all eight positions.

VI. Conclusion

We have presented a pneumatic haptic wristband that can render local pressure and vibration at eight locations around the wrist. We have demonstrated forces of over 10 N and maximum displacements of over 10 mm for each bellow at 100 kPa. We found that each TPU bellow acts as a spring with a stiffness that increases with increasing pressure and provided model parameters specific to our design. Fitting exponential curves to system pressure responses yields time constants of under 40 ms across the entire workspace of the device, not including delays of roughly 10 ms associated with valve commands and longer delays associated with regulator control.

Future work includes exploring different means of evaluating and improving the functionality of this device. Although we measured the forces this wristband can deliver, more work is needed to understand how these forces are perceived by humans. Such studies could provide meaningful feedback as to what combinations of pressure and vibration are most effective for various concepts important to AR/VR, such as a sense of presence or location perception of various cues.

We are also interested in allowing input from the user to the system, through sensing elements in each bellow, and early efforts have shown the potential of embedding a

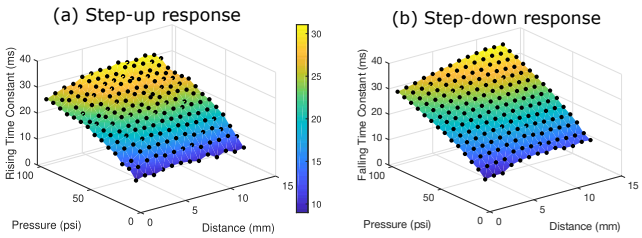

Fig. 9: We estimated time constants, as given in Equations. (4)-(5) for bellow pressure responses to steps from (a) 0 kPa to 100 kPa and from (b) 100 kPa to 0 kPa across the workspace of the device. Dots are experimental data and surfaces are interpolated between collected data.

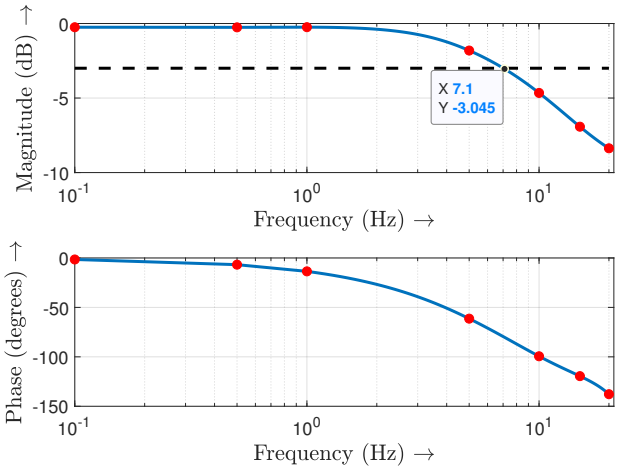

Fig. 10: Bode plot of output bellow force to an input pressure between 0 kPa and 100 kPa. Dots are experimental measurements made at [0.1, 0.5, 1, 5, 10, 15, 20] Hz, and lines are spline interpolations between points.

force sensor to detect "clicks". Other areas of exploration include tracking the wristband and modeling other design parameters, such as shape and size of each bellow layer.

REFERENCES

[1] C. Pacchierotti, *et al.*, "Wearable haptic systems for the fingertip and the hand: Taxonomy, review, and perspectives," *IEEE Transactions on Haptics*, vol. 10, no. 4, pp. 580–600, Oct. 2017.

[2] J. Perret and E. Vander Poorten, "Touching virtual reality: a review of haptic gloves," June 2018.

[3] I. Oakley, *et al.*, "Determining the feasibility of forearm mounted vibrotactile displays," in *14th Symp. on Haptic Interfaces for Virtual Environment and Teleoperator Sys.*, Mar. 2006, pp. 27–34.

[4] M. Matscheko, *et al.*, "Tactor placement in wrist worn wearables," in *Intl. Symp. on Wearable Computers (ISWC)*, Oct. 2010, pp. 1–8.

[5] H. Chen, *et al.*, "Tactor localization at the wrist," in *Haptics: Perception, Devices and Scenarios, 6th Intl. Conf., EuroHaptics, Proc.*, June 2008, pp. 209–218.

[6] J. Hong, *et al.*, "Evaluating angular accuracy of wrist-based haptic directional guidance for hand movement," in *Proc. of the 42Nd Graphics Interface Conf.* Canadian Human-Computer Communications Society, 2016, pp. 195–200.

[7] A. A. Stanley and K. J. Kuchenbecker, "Evaluation of tactile feedback methods for wrist rotation guidance," *IEEE Transactions on Haptics*, vol. 5, no. 3, pp. 240–251, Mar. 2012.

[8] E. Treadway, *et al.*, "The role of auxiliary and referred haptic feedback in myoelectric control," in *IEEE World Haptics Conf. (WHC)*, June 2015, pp. 13–18.

[9] J. D. Brown, *et al.*, "A wrist-squeezing force-feedback system for robotic surgery training," in *IEEE World Haptics Conf. (WHC)*, June 2017, pp. 107–112.

[10] L. Meli, *et al.*, "The hbracelet: A wearable haptic device for the distributed mechanotactile stimulation of the upper limb," *IEEE Robotics and Automation Letters*, vol. 3, no. 3, pp. 2198–2205, July 2018.

[11] M. Aggravi, *et al.*, "Design and evaluation of a wearable haptic device for skin stretch, pressure, and vibrotactile stimuli," *IEEE Robotics and Automation Letters*, vol. 3, no. 3, pp. 2166–2173, July 2018.

[12] N. Dunkelberger, *et al.*, "Conveying language through haptics: A multi-sensory approach," in *Proc. of the 2018 ACM Intl. Symp. on Wearable Computers*. New York, NY, USA: ACM, 2018, pp. 25–32.

[13] H. Pohl, *et al.*, "Squeezeback: Pneumatic compression for notifications," in *Proc. of the CHI Conf. on Human Factors in Computing Systems*. New York, NY, USA: ACM, 2017, pp. 5318–5330.

[14] R. Kettner, *et al.*, "Towards pressure-based feedback for non-stressful tactile notifications," in *Proc. of the 19th Intl. Conf. on Human-Computer Interaction with Mobile Devices and Services*. New York, NY, USA: ACM, 2017, pp. 89:1–89:8.

[15] B. Stephens-Fripp, *et al.*, "Applying mechanical pressure and skin stretch simultaneously for sensory feedback in prosthetic hands," in *7th IEEE Intl. Conf. on Biomedical Robotics and Biomechatronics (Biorob)*, Aug 2018, pp. 230–235.

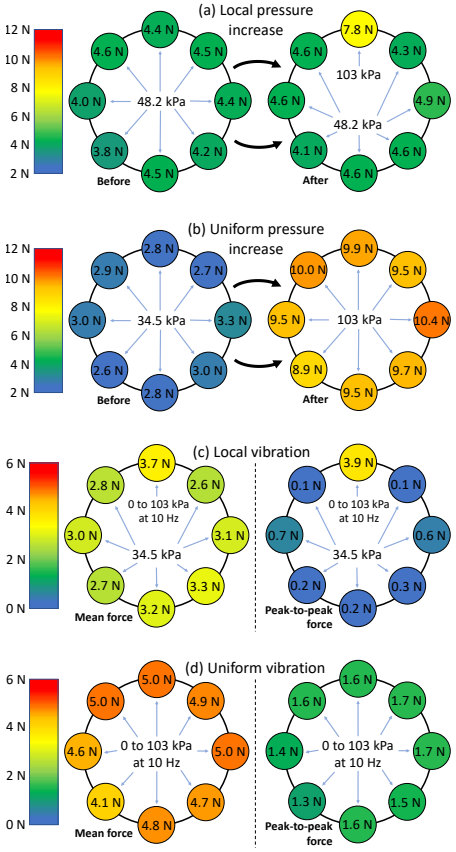

Fig. 11: We recorded normal force under each bellow during different haptic cues, including (a) pressure increase in one bellow, (b) pressure increase in all bellows, (c) vibration in one bellow, and (d) vibration in all bellows. The measured normal forces are shown in the small circles used to represent bellows, and the blue arrows indicate commanded pressure. Note that in (a) and (b) the commanded pressure changes between diagrams, whereas the diagrams in (c) and (d) represent the same vibrotactile command.

[16] L. He, *et al.*, "Pneuhaptic: Delivering haptic cues with a pneumatic armband," in *Proc. of the ACM Intl. Symp. on Wearable Computers*. New York, NY, USA: ACM, 2015, pp. 47–48.

[17] M. Raitor, *et al.*, "Wrap: Wearable, restricted-aperture pneumatics for haptic guidance," in *IEEE Intl. Conf. on Robotics and Automation (ICRA)*, May 2017, pp. 427–432.

[18] G. Dmmer, *et al.*, "Design and shape optimization of polyjet bellows actuators," in *IEEE Intl. Conf. on Soft Robotics (RoboSoft)*, April 2018, pp. 282–287.

[19] H. Sonar and J. Paik, "Soft pneumatic actuator skin with piezoelectric sensors for vibrotactile feedback," *Frontiers in Robotics and AI*, vol. 2, p. 38, Jan. 2016.

[20] A. B. Lawrence, *et al.*, "Mechanical implementation of a variable-stiffness actuator for a softly strummed ukulele," in *IEEE/RSJ Intl. Conf. on Intelligent Robots and Systems (IROS)*, Oct 2016, pp. 376–382.

[21] L. Yao, *et al.*, "Pneui: Pneumatically actuated soft composite materials for shape changing interfaces," in *Proc. of the 26th Annual ACM Symp. on User Interface Software and Tech.* ACM, 2013, pp. 13–22.

[22] R. V. Martinez, *et al.*, "Elastomeric origami: Programmable paper-elastomer composites as pneumatic actuators," *Advanced Functional Materials*, vol. 22, no. 7, pp. 1376–1384.

[23] S. Li, *et al.*, "Fluid-driven origami-inspired artificial muscles," *Proc. of the National Academy of Sciences*, vol. 114, no. 50, pp. 13 132–13 137, 2017.

[24] T. Ranzani, *et al.*, "Deployable stabilization mechanisms for endoscopic procedures," in *IEEE Intl. Conf. on Robotics and Automation (ICRA)*, May 2017, pp. 1125–1131.

[25] S. Becker, *et al.*, "Pop-up tissue retraction mechanism for endoscopic surgery," in *IEEE/RSJ Intl. Conf. on Intelligent Robots and Systems (IROS)*, Sep. 2017, pp. 920–927.